PHYSICAL ACOUSTICS

Nonlinear Spherically Divergent Shock Waves Propagating in a Relaxing Medium[1]

P. V. Yuldashev[a], M. V. Averiyanov[a], V. A. Khokhlova[a], S. Ollivier[b], and Ph. Blanc-Benon[b]

[a] *Faculty of Physics, Moscow State University, Vorob'evy gory, Moscow, 119992 Russia*
e-mail: vera@acs366.phys.msu.ru
[b] *LMFA, UMR CNRS 5509, Ecole Centrale de Lyon, 69134 Ecully Cedex, France*
e-mail: Philippe.Blanc-Benon@ec-lyon.fr
Received January 11, 2007

Abstract—The propagation of nonlinear spherically diverging *N*-waves in atmosphere was studied experimentally and theoretically. The relative effects of nonlinear, dissipation, and relaxation phenomena on the *N*-wave duration and amplitude were investigated based on the numerical solutions of the modified Burgers equation. It is shown that, under the experimental conditions, the duration of a pulse increases mainly due to nonlinear propagation, whereas the amplitude depends on the combined effects of nonlinearity, dissipation, and relaxation. The frequency response of the measuring system is obtained. The calibration of the amplitude and duration of the experimental waveforms is performed based on the nonlinear lengthening of the propagating pulse. The results of numerical modeling show good agreement with experimental data.

1. INTRODUCTION

Shock wave propagation in atmosphere is an important subject of recent experimental and theoretical acoustic research [1–3]. Intensive studies of this problem were started due to rapidly growing interest in supersonic civil aviation, which is inseparably related to the problems of sonic boom propagation in the atmosphere. Sonic booms, i.e., intense shock waves generated by supersonically moving aircraft, propagate in the atmosphere towards the ground and form an acoustic field with a nonuniform acoustic pressure distribution [4]. High and low pressure levels may affect human beings and even buildings. To estimate the possible effect of the sonic boom, it is necessary to predict the *N*-wave characteristics, such as peak and average pressure, pulse duration, and shock rise time. The temporal parameters and spatial structure of the acoustic field produced by sonic boom close to the earth strongly depend on the atmospheric conditions, pulse scattering by the atmosphere inhomogeneities, relaxation, and nonlinear propagation effects, and are also influenced by the aircraft trajectory. The turbulent layer of the atmosphere changes the acoustic field creating additional focusing zones [5]. A complete theoretical investigation of nonlinear sonic boom propagation is a very difficult problem, and, therefore, most of the theoretical results to date were obtained within simplified models like geometrical acoustics [6] and parabolic approximation [1, 7, 8].

Experimental studies of real sonic booms are difficult due to the high costs and the lack of control of the outdoor measurements. The experimental focus therefore has turned to the laboratory-scale measurements, which proved to be a good alternative to the field measurements. The results have been reported by several authors, who used electrical spark sources [3, 9, 10] or lasers [2] to generate high-amplitude acoustic shock *N*-waves. Since the turbulent fields and the sources can be better controlled in laboratory environment, it gives an opportunity for more accurate investigations [3, 11].

In the present paper, a laboratory-scale experimental setup utilizing an electrical spark source is presented. The setup allows to generate short-duration (30 μs) and high-amplitude (1000 Pa at 15 cm from the source) spherically divergent *N*-waves with good reproducibility. It was designed and built with the goal to study the processes of sonic boom propagation through the turbulent layer with or without account of the boundary effects. At the first step, the experiments and simulations were performed in a homogeneous atmosphere in order to calibrate the measurement track, to validate the modeling approach vs. experiment, and to better understand the effects of relaxation, thermoviscous absorption, and acoustic nonlinearity on the *N*-wave distortion. Shock waveforms were measured up to distances of 2 m from the source with a 1/8-inch microphone of 150-kHz bandwidth. The modified Burgers equation that includes the combined effects of spherical spreading of the wave, nonlinear waveform distortion, thermoviscous dissipation, and N_2 and O_2 relaxation effects

---

[1] The article was translated by the author (V.A. Khokhlova).

was employed in the simulations. The initially ideal *N*-waveform was used as a boundary condition given at some distance from the source. A time-domain numerical algorithm was developed to simulate the *N*-wave propagation.

2. THEORY

2.1. The Propagation Model

The Burgers equation, extended to include relaxation processes and spherical divergence of a nonlinear wave in a homogeneous medium can be written in the form [12]

$$\frac{\partial p}{\partial r} + \frac{p}{r} = \frac{\varepsilon}{\rho_0 c_0^3} p \frac{\partial p}{\partial \tau} + \frac{b}{2\rho_0 c_0^3} \frac{\partial^2 p}{\partial \tau^2}$$
$$+ \sum_{v=1}^{M} d_v \frac{\partial}{\partial \tau} \int_{-\infty}^{\tau} \exp(-(\tau - \tau')/\tau_v) \frac{\partial p}{\partial \tau'} d\tau'. \tag{1}$$

Here, p is the acoustic pressure, r is the radial propagation coordinate, $\tau = t - (r - r_0)/c_0$ is the retarded time, c_0 is the ambient sound speed at low frequencies, r_0 is the reference distance at which the boundary conditions are set, ρ_0 is the air density, ε is the coefficient of nonlinearity in air, b is the coefficient of viscosity, and M is the total number of relaxation processes. Each vth relaxation process is characterized by two parameters: relaxation time τ_v and coefficient $d_v = (c_\infty^v - c_0)/c_0^2 = c_v/c_0^2$,

where c_∞^v is the so-called frozen sound speed of acoustic signal propagation through the medium with relaxation time much longer than the effective duration of the signal $T_s \ll \tau_v$. The second term on the left-hand side of Eq. (1) is responsible for the spherical divergence of the wave, while the right-hand side includes nonlinear effects (the first term), dissipation due to thermoviscous absorption of the medium (the second term), and relaxation processes (the last term) associated with the excitation of oscillatory energy levels of molecules in the medium [12–14]. For Eq. (1) to be valid, it is necessary, that $\lambda/r \ll 1$. This condition holds for the laboratory-scale experiments at hand ($\lambda \sim 15$ mm, $r > 150$ mm).

The number of relaxation processes M in Eq. (1) is equal to the number of molecule types in the propagation medium. The atmosphere consists mainly of nitrogen and oxygen molecules, which define its relaxing properties and the corresponding frequency dependence of the sound speed and absorption [12, 14]. The effect of relaxation on the waveform distortion therefore will strongly depend on the frequency content of the shock waves generated in laboratory experiments. The shock waveform and the corresponding frequency spectrum that will be further used in simulations as a boundary condition given at the distance r_0 from the source are shown in Figs. 1a and 1b. The waveform is

an ideal *N*-shape pulse with an infinitely short rise time and the main parameters, i.e., duration (30 μs) and amplitude (1000 Pa), close to those measured experimentally at the nearest distance to the source $r_0 = 15$ cm. The characteristic relaxation frequencies of oxygen ($f_1 = 1/(2\pi\tau_1) \sim 26500$ Hz) and nitrogen ($f_2 = 1/(2\pi\tau_2) \sim 300$ Hz) molecules were calculated according to the humidity (34%) and temperature (20°C) of the experimental conditions and are shown in Figs. 1b–1d as vertical dotted lines [14]. The relaxation frequency of oxygen lies near the maximum of the *N*-wave spectrum, while the nitrogen frequency corresponds to the nearly zero part of the spectrum at low frequencies. The nitrogen relaxation process thus should have very little effect on the shock wave propagation. The frequency dependence of the sound speed c and absorption α, which incorporate the effects of relaxation, can be obtained from the linearized Eq. (1) [12]:

$$c = c_0 \left[1 + c_0 \sum_{v=1}^{2} \frac{d_v (\omega\tau_v)^2}{1 + (\omega\tau_v)^2} \right],$$
$$\alpha = \frac{b\omega^2}{2\rho_0 c_0^3} + \sum_{v=1}^{2} \frac{d_v}{\tau_v} \frac{(\omega\tau_v)^2}{1 + (\omega\tau_v)^2}. \tag{2}$$

These dependences are shown in Figs. 1c and 1d, respectively. The presence of relaxation will change the wave amplitude due to additional absorption, and also change the arrival time of the pulse, since the shock front is formed of high frequencies propagating faster than the ambient sound speed c_0. The effect of nitrogen on arrival time and amplitude is expected to be negligible in comparison with that of oxygen. The sound speed variation due to N_2 relaxation is about 5 times smaller than that introduced due to O_2 relaxation (Fig. 1c), and the effective increase in absorption for nitrogen N_2 is three orders of magnitude smaller than that for oxygen O_2 (Fig. 1d).

2.2. The Numerical Algorithm

To perform numerical simulations, it is convenient to rewrite Eq. (1) in nondimensional form:

$$\frac{\partial P}{\partial \sigma} = P\frac{\partial P}{\partial \theta} + \frac{1}{\Gamma} \exp\left(\frac{x_s}{r_0}\sigma\right) \frac{\partial^2 P}{\partial \theta^2}$$
$$+ \sum_{v=1}^{2} D_v \exp\left(\frac{x_s}{r_0}\sigma\right) \frac{\partial}{\partial \theta} \int_{-\infty}^{\theta} \exp\left(-\frac{\theta - \theta'}{\theta_v}\right) \frac{\partial P}{\partial \theta'} d\theta'. \tag{3}$$

Here, $P = pr/(p_0 r_0)$ is the dimensionless sound pressure, $\sigma = r_0 \ln(r/r_0)/x_s$ is the spatial dimensionless propagation coordinate, $x_s = \rho_0 c_0^3 T_0/\varepsilon p_0$ is the characteristic nonlinear distance; $\theta = \tau/T_0$ is the dimensionless time, $\Gamma = 2\varepsilon p_0 T_0/b$ is the Goldberg number determining the relative effect of nonlinearity and thermoviscous absorption; $\theta_v = \tau_v/T_0$ is the dimensionless relaxation time,
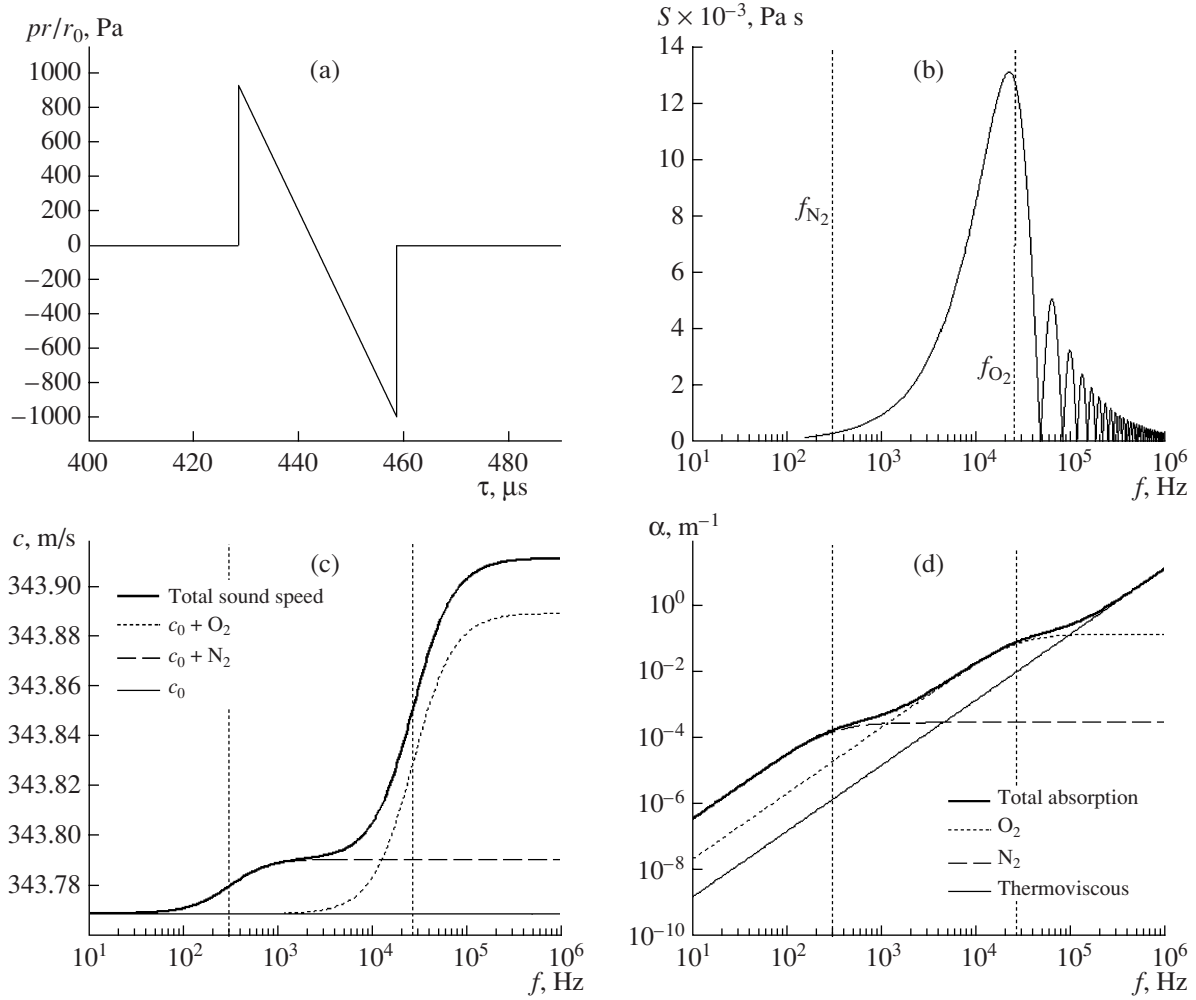
Fig. 1. (a) Initial *N*-pulse waveform and (b) its spectrum. Dependence of the (c) sound speed and (d) absorption on frequency due to relaxation in atmosphere. The characteristic relaxation frequencies of oxygen O_2 and nitrogen N_2 are shown by vertical dotted lines.

and $D_v = \rho_0 c_0^3 d_v / \varepsilon p_0 = \rho_0 c_0 c_v / \varepsilon p_0$ is the dimensionless relaxation coefficient for the processes $v = 1, 2$. To avoid limitations of validity in the model, we retain both oxygen and nitrogen relaxation effects in Eq. (3) and in further numerical simulations. The waveform parameters measured at the closest distance r_0 from the source, such as the peak positive pressure p_0 and the half-duration T_0, were chosen to be the reference values.

To obtain a solution for the dimensionless pressure P, Eq. (3) was solved numerically in the time domain using an operator splitting procedure. At each grid step in propagation distance σ, the equation was divided into three physically consistent equations describing different physical effects:

nonlinearity

$$\frac{\partial P}{\partial \sigma} = \frac{1}{2}\frac{\partial P^2}{\partial \theta}, \qquad (4)$$

thermoviscous absorption

$$\frac{\partial P}{\partial \sigma} = \frac{1}{\Gamma}\exp\left(\frac{x_s}{r_0}\sigma\right)\frac{\partial^2 P}{\partial \theta^2}, \qquad (5)$$

and relaxation

$$\frac{\partial P}{\partial \sigma} = \sum_{v=1}^{2} D_v \exp\left(\frac{x_s}{r_0}\sigma\right)\frac{\partial}{\partial \theta}\int_{-\infty}^{\theta}\exp\left(-\frac{\theta - \theta'}{\theta_v}\right)\frac{\partial P}{\partial \theta'}d\theta'. \qquad (6)$$

Here, the simple wave equation (4) is written in the flux-conservative form.

At the first step of the algorithm, the nonlinear effects, Eq. (4), are taken into account using the central flux-conservative scheme of the second-order accuracy in time and the first-order accuracy in propagation coordinate [15]. This scheme has a small internal viscosity, and it is sufficient to have only 2–3 time points per shock to describe its evolution with high accuracy and stability without introducing additional physical

absorption to suppress the high frequencies. At the second step, thermoviscous dissipation effects, Eq. (5), are included using the explicit central finite-difference scheme. And at the last step of numerical procedure, the relaxation, Eq. (6), is modified following the approach presented in [13]:

$$\left(\frac{1}{\theta_v} + \frac{\partial}{\partial\theta}\right)\frac{\partial P}{\partial\sigma} = D_v \exp\left(\frac{x_s}{r_0}\sigma\right)\frac{\partial^2 P}{\partial\theta^2}. \qquad (7)$$

Equation (7) is then calculated using the Crank–Nicholson algorithm of the second-order accuracy in time θ and spatial propagation coordinate σ.

To validate the algorithm of modeling the nonlinear operator, numerical and analytical solutions to the simple wave equation were compared for an ideal N-wave propagation [12]. To validate the accuracy of the combined nonlinear and relaxation modeling, the numerical results were compared with the stationary Polyakova solution for a monorelaxing medium [16]. For the following computational steps: $\Delta\sigma = 0.002$ and $\Delta\theta = 0.0262$, the maximum error in numerical solution, as compared to the analytic results, was less than 1%.

2.3. Results

For the numerical simulations of nonlinear N-wave propagation in a relaxing medium, the specific parameters of the medium corresponding to those of the laboratory-scale experiment were set: $\varepsilon = 1.21$, $b = 4.86 \times 10^{-5}$ Pa s, $\rho_0 = 1.29$ kg/m^3, and $c_0 = 343.77$ m/s. The parameters of the relaxation processes were calculated using empirical expressions for the relative humidity 34%, temperature 293 K, and an ambient pressure level of 1 atmosphere: $c_1 = 0.11$ m/s, $\tau_1 = 6.0$ μs (O$_2$), $c_2 = 0.023$ m/s, and $\tau_2 = 531$ μs (N$_2$) [14]. The boundary condition was set at the distance $r_0 = 15$ cm as an ideal N-pulse with characteristic experimental values of amplitude $p_0 = 1000$ Pa and half-duration $T_0 = 15$ μs (Fig. 1a). The corresponding values of nondimensional parameters in Eq. (3) are as follows: $\Gamma = 746.9$, $D_1 = 0.04$, $D_2 = 8.43$, $\theta_1 = 0.4$, $\theta_2 = 35.4$, and $x_s/r_0 = 4.33$.

To illustrate the relative effects of nonlinearity, thermoviscous absorption, and relaxation under experimental conditions, the shock waveforms were calculated numerically at the distance $r = 6$ m from the source assuming different regimes of propagation (Fig. 2). Various physical effects were alternately included into the model. Linear propagation in an ideal medium was considered first, then only acoustic nonlinearity was included, then relaxation effects only, thermoviscous absorption only, and finally, all the above-mentioned effects. In order to "exclude" the spherical divergence of the wave, the sound pressure in all solutions was multiplied by the ratio of the current propagation distance to the initial one $r_0 = 15$ cm from the source. If only the divergence of the wave is taken into account in simulations ("no effects", the grey solid line), the corrected waveform does not change with the
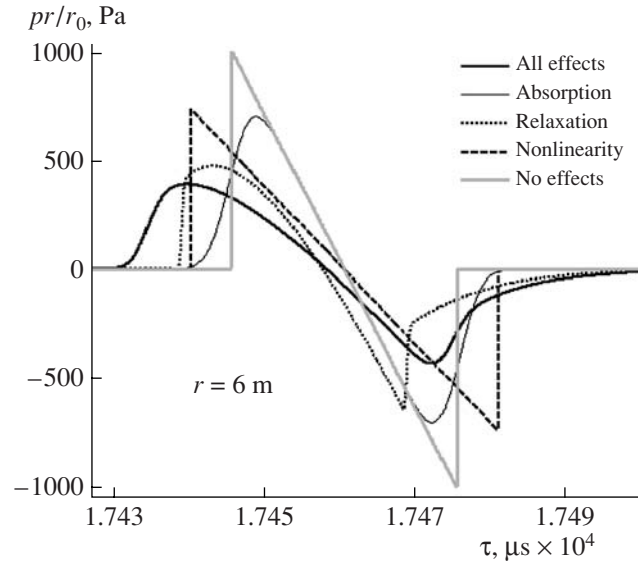
Fig. 2. N-pulse waveforms calculated at the distance $r = 6$ m from the source with alternate account for different physical effects: ideal linear medium (no effects, the grey solid line), nonlinearity only (the dashed line), relaxation only (the dotted line), thermoviscous absorption only (the thin black line), and all the effects together (the black line). The waveforms are multiplied by the ratio r/r_0 to exclude spherical divergence of the wave.

propagation distance and, thus, coincides with the initial waveform shown in Fig. 1a. The nonlinear propagation (the dashed line) results in the classical lengthening of the N-pulse and the corresponding decrease in the shock amplitude [12]. Relaxation processes (the dotted line) lead to an asymmetric waveform distortion and a displacement of both front and distal shocks towards the direction of propagation. The peak value of the rounded positive waveform cycle is reduced more than the peak value in the sharp negative tail of the pulse. The pulse length between the front and distal shock fronts, however, does not noticeably change due to relaxation as both shock fronts move with the same speed of high frequencies. The sharp structure of shock fronts is also not strongly affected by relaxation. Thermoviscous absorption substantially reduces the shock amplitude and broadens the shock front without changing the symmetry of the pulse and its duration between the half-peak pressure levels (the thin black solid line). It is seen that all the physical effects, i.e., nonlinearity, relaxation, and thermoviscous absorption, are of comparable importance in reducing the pulse amplitude and thus should all be taken into account in theoretical modeling. The solution corresponding to this case of "all effects" included in the model is shown as a thick black solid line. The contributions of different physical effects to the pulse distortion now are clearly seen from the preceding auxiliary cases. The peak pressure values are determined by nonlinearity, relaxation, and thermoviscous absorption in comparable extent. The asymme-
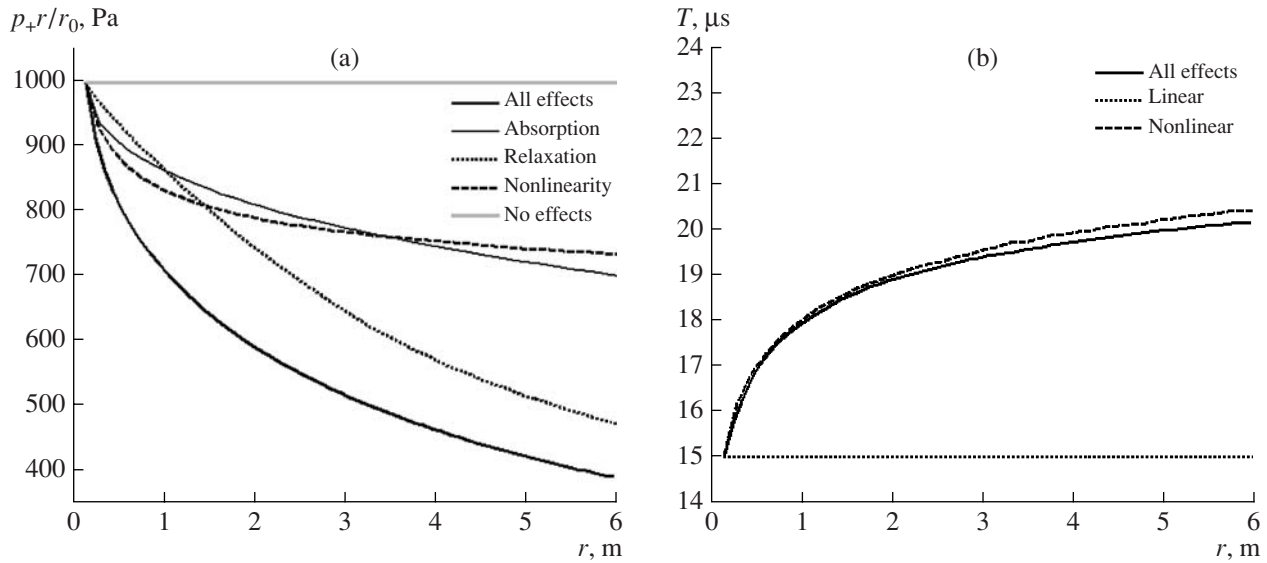
Fig. 3. Dependence of the (a) peak positive pressure and (b) half-duration of the *N*-pulse on the propagation distance. The peak positive pressure p_+ is multiplied by the ratio r/r_0 to exclude spherical divergence of the wave.

try of the waveform is due to relaxation, and the shock broadening is due to thermoviscous absorption. The pulse duration increases due to nonlinear propagation. Since nonlinear effects depend on the initial pulse amplitude, this effect gives an opportunity for an absolute calibration of the microphone sensitivity based on the measured pulse lengthening at different distances [10].

The relative effects of nonlinearity, relaxation, and absorption on the peak positive pressure p_+ and half-pulse duration T over the propagation path are shown in more detail in Fig. 3. It is seen that, for the peak pressure p_+, nonlinear effects predominate over the relaxation and absorption in diminishing the pulse amplitude up to a distance of approximately 2 m from the source (Fig. 3a). Beyond this distance, nonlinear absorption on the shocks becomes much lower as the shock amplitude decreases due to spherical divergence of the pulse, and the relaxation and absorption effects therefore begin to predominate.

Figure 3b shows the results of simulations for the half-pulse duration T versus the propagation distance r. Since the N-waveform is strongly asymmetric, it is difficult to determine its duration correctly in the time domain. Moreover, in the case of experimental data, the waveforms could be strongly affected by the microphone response and by the diffraction by the edges of the microphone. Here, we propose to determine the duration of the pulse in the frequency domain by matching the positions of the minima in the calculated or measured pulse spectrum with those in the spectrum of an ideal N-wave with an infinitely thin front (Figs. 1a and 1b). This determination relies on the assumption that all linear waveform distortions additional to nonlinear lengthening can be represented as multiplication

of the pulse spectrum by a transfer function that changes smoothly with frequency and does not shift zero values of the N-wave amplitude spectrum and, consequently, these minima. In contrast to the peak positive pressure, which was significantly affected by both nonlinear and relaxation/absorption effects, the pulse duration changes mainly due to the nonlinear propagation of shock fronts. A small influence of the relaxation/absorption processes is observed due to the suppression of nonlinear effects by lowering the pulse peak pressure values. However, this influence is almost negligible (Fig. 3b). The characteristic scale of nonlinear propagation can also be defined here as an interval with the high gradient of the pulse lengthening curve and is about 2 m as well. Note that the characteristic nonlinear distance estimated here is only applicable to the current experimental conditions, pulse amplitude, and duration.

3. EXPERIMENTAL METHODS

The experimental setup is schematically represented in Fig. 4. It basically includes an electric spark source to generate short spherically divergent acoustic N-pulses, a microphone to measure the pulse waveform at certain distances from the source, an amplifier, and an oscilloscope to record the signal. The source and the microphone were mounted on a rail to provide the possibility of changing the distance between them. An additional reference microphone (not shown in the diagram) with a fixed position of 37 cm above the source was used to control the stability of the shape and peak characteristics of the propagating shock wave. Acoustic measurements of shock pulses were performed in homogeneous ambient air, in an anechoic chamber, at distances from 15 cm to 2 m from the spark source.

To produce an electric spark, a high voltage (15 kV) was applied between tungsten electrodes with a 6-mm gap. The electric discharge creates a sudden local heating of the gas between the electrodes, which generates a short-duration but high-amplitude pressure perturbation. This perturbation has a complex shape that varies from one spark to another. However, since the pressure amplitude of the pulse is very high ($\gg$1000 Pa), the initial waveform transforms into an N-wave due to nonlinear effects within the first centimeters of propagation. The experiments showed a good reproducibility of the N-wave parameters: the peak positive pressure measured by the reference microphone was 390 ± 10 Pa, the pulse half-duration was 15.27 ± 0.23 μs, and the standard deviation of arrival time was 1.7 μs. At a distance of 1 m from the source, the typical maximum pressure amplitude P_{max} was 120 Pa, the half-duration T was 17.2 μs, and the shock rise time t_{10-90}, which was determined as the interval between the peak pressure increase from 10% to 90% of P_{max}, was less than 3 μs.

High-frequency broadband microphones (B&K) of 1/8-inch diameter were used in the experiments without a grid to avoid diffraction effects. The microphones were mounted in a baffle in order to postpone the diffracted waves, because the size of the microphone membrane was on the same order of magnitude as the shortest wavelengths of the acoustic signal [3, 9]. The microphone electric output was amplified by a B&K Nexus amplifier, which was modified to extend its bandwidth up to 200 kHz. The amplifier output was digitally recorded by the data acquisition card at a sampling frequency of 5 MHz.

4. THE COMPARISON OF NUMERICAL AND EXPERIMENTAL DATA

To simulate the experiment, an ideal N-waveform was taken as a boundary condition at the distance of the first measured waveform $r_0 = 0.15$ m. The initial amplitude and duration of the N-wave were obtained by matching the duration of pulses measured at various distances from the source and those predicted theoretically at the same distances. The duration of pulses in both cases was calculated from the position of nulls in their spectra as discussed earlier in the paper (Sect. 2.3). For theoretical predictions, the dependence of the normalized pulse half-duration Ξ versus the propagation distance was obtained from the exact analytic solution to the simple wave equation (4):

$$\Xi = \sqrt{1 + \sigma} \qquad (8)$$

or, in dimensional coordinates,

$$T = T_0 \sqrt{1 + \frac{\varepsilon}{\rho_0 c_0^3} \frac{p_0}{T_0} r_0 \ln\left(\frac{r}{r_0}\right)}. \qquad (9)$$

Here, we rely on the results shown in Fig. 3b that the change in the pulse duration was mainly due to nonlinear effects, rather than relaxation or absorption. Two
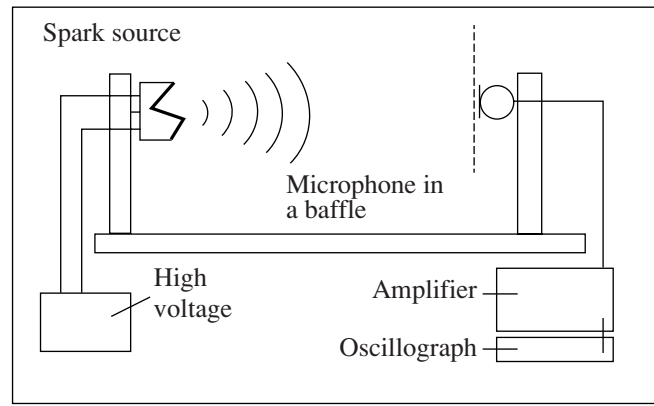
Fig. 4. Schematic diagram of the experimental setup.

unknown parameters, T_0 (the initial half-duration) and p_0 (the peak pressure), in the linear dependence of T^2 on $\ln(r/r_0)$ in solution (9) were obtained by fitting the experimental values [10]. For this purpose, the least squares method was used. The determination of the initial N-wave parameters using this method showed good accuracy as soon as the correlation coefficient was $R = 0.975$. The initial half-duration was found to be $T_0 = 14.32$ μs, and the peak positive pressure was $p_0 = 1148$ Pa at the distance $r_0 = 0.15$ m from the source. For these parameters of the experiment, the nondimensional coefficients in Eq. (3) are: $\Gamma = 857.4$, $D_1 = 0.035$, $D_2 = 7.34$, $\theta_1 = 0.419$, $\theta_2 = 37.08$, and $x_s/r_0 = 3.77$.

The measured and calculated waveforms are presented in Figs. 5a and 5b at the radial distances $r = 0.15$, 0.3, 0.5, 1, 1.5, and 2 m, which in the case of the experiment were measured with a ± 3 mm error. The experimental waveforms have a much more complex structure with several oscillations on the back slope, as compared to the calculated N-waves. The rise times of the measured shock fronts are much longer than those of the calculated ones. These differences between experimental and simulation results can be attributed to the microphone and amplifier limited frequency response and to the diffraction effects at the edges of the baffle and microphone, since there was still a small gap between them.

To provide better agreement between the experimental and numerical waveforms, it is necessary to know the total frequency response of the measurement system, which includes microphone filtering, response of the amplifier, and diffraction effects. The total frequency response was calculated here as the ratio between the complex spectra of the pulses measured and calculated at the same distances from the source. The resulting amplitude frequency response is presented in Fig. 6 (the solid line) and compared with the frequency response of the microphone itself obtained from the manufacturer datasheet (the dotted line). It is seen that the total system response is flat up to 10 kHz, then continues with some ± 4 dB oscillations, and ends
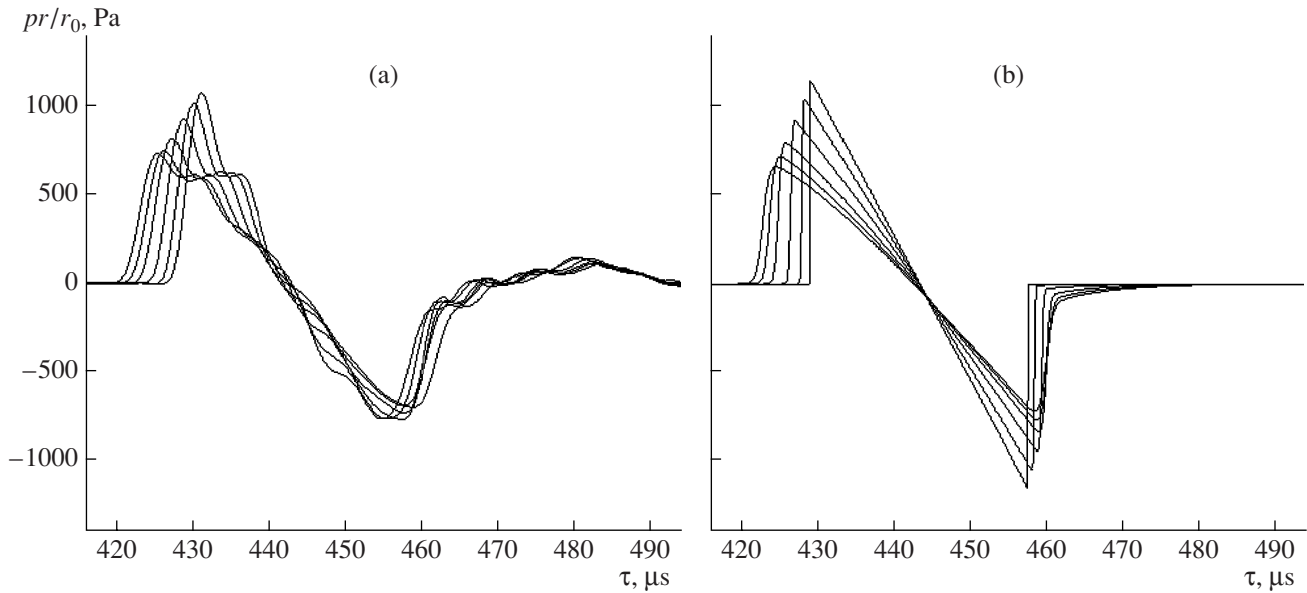
Fig. 5. (a) Measured and (b) calculated *N*-waves at different distances from the source: 0.15, 0.3, 0.5, 1, 1.5, and 2 m. The monotonic decrease in the pulse amplitude corresponds to the increase in the propagation distance.

with the frequency cutoff at about 150–200 kHz. The structures of the curves of both filters, which were calculated and provided by the manufacturer, are pretty close to each other. The difference between the curves on the plateau is less than 1 dB. The distortions of the measured waveforms are, therefore, mainly due to the frequency response of the microphone. Additional oscillations (compared to the microphone response) at frequencies higher than 10 kHz are due to the waves
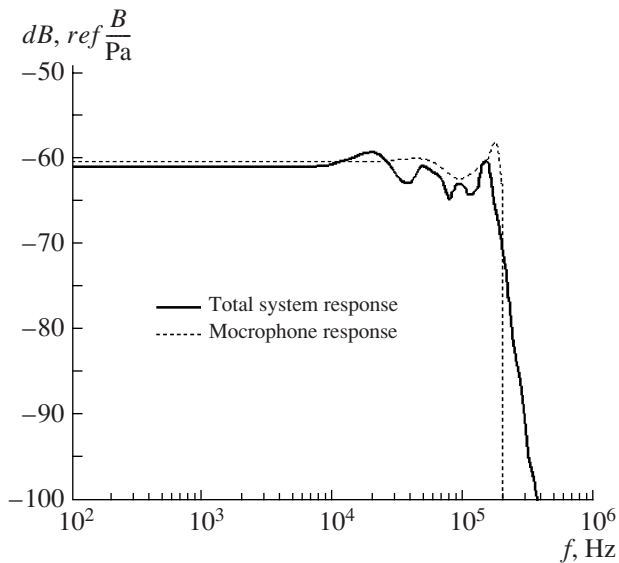

Fig. 6. Amplitude–frequency response calculated for the total measuring system (the solid line) and the response of the microphone provided by the manufacturer (the dotted line).

diffracted by the baffle edges. The phase frequency filter of the system is not employed here, as it showed insufficient stability from pulse to pulse (zero plateau up to 10 kHz and variety of oscillations after that) due to random fluctuations in the spark positions and, therefore, in the pulse arrival time.

Figure 7a shows the experimental waveform measured at the distance $r_0 = 0.15$ m from the source (the dotted line), the initial ideal *N*-wave (the thick solid line), and the initial *N*-wave filtered (the thin solid line) with the calculated amplitude response. It is seen that, after filtering, the ideal *N*-wave with an infinitely small rise time and a high peak positive pressure transforms to a waveform with a shape and peak positive pressure much closer to the experimental ones. However, there is still a difference in the peak negative pressure level, which could be explained by the fact that we did not take into account the phase characteristics of the measuring system response. The oscillating structure and disturbances before the shock front are also due to the filtering artifacts. The frequency spectra that correspond to the presented waveforms are shown in Fig. 7b. Good agreement between the positions of spectrum minima is achieved in all three cases. Note, that, as was discussed earlier in the paper, the filtering does not change these positions and, thus, the characteristic duration of the pulse.

The waveforms measured and calculated at the distance *r* = 1.5 m from the source are compared in Fig. 7c. It is seen that the peak pressure values, both positive and negative, are close to each other for all three waveforms, including the filtered one. However, a strong difference in the steepness (rise time) of the shock front is observed between the experimental pulse and the theo-
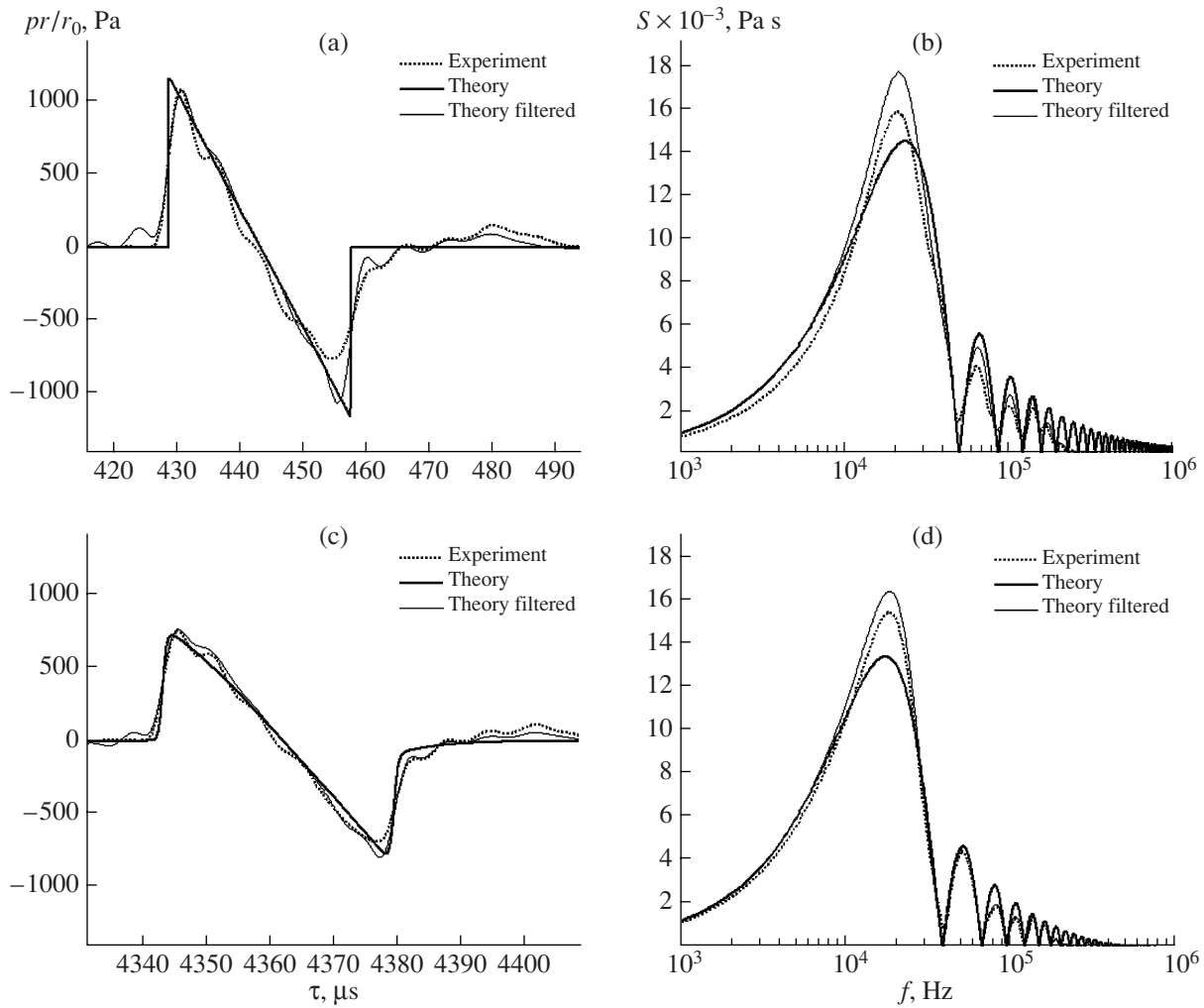
Fig. 7. Experimental (the dotted line) and theoretical (the thick solid line) N-pulse waveforms and the corresponding spectra at the (a, b) initial distance $r_0 = 0.15$ m and (c, d) $r = 1.5$ m from the source. The filtered theoretical waveforms and their spectra are shown by the thin solid lines.
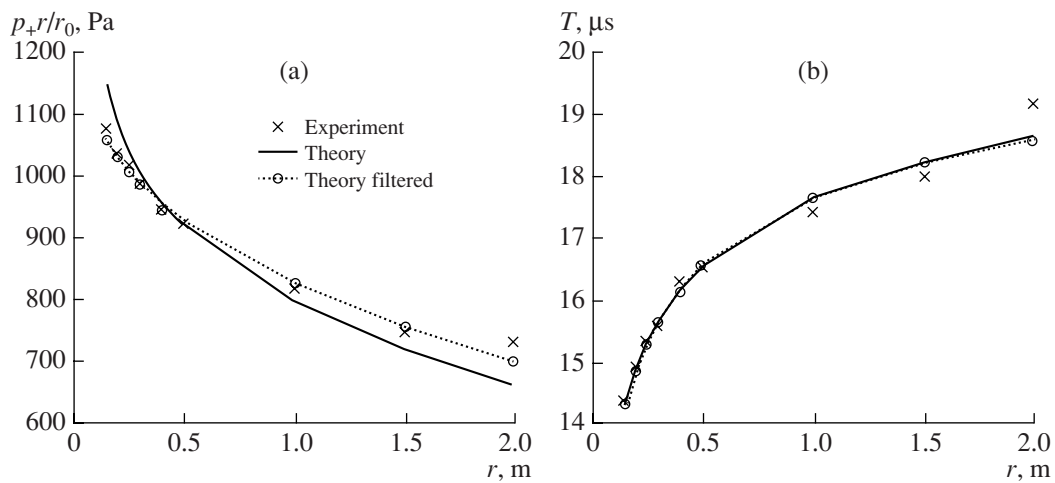
Fig. 8. Dependence of the (a) peak positive pressure and (b) half-duration of the wave on the propagation distance. The solid line shows the calculated waveform, the crosses show the measured waveform, and the circles, the filtered theoretical waveform.

retical one simulated without further filtering. Application of the amplitude filtering to the calculated waveform results in a much better agreement in the rise time with the experiment (the solid thin line and the dotted line). The shock front steepness of the filtered numerical signal almost coincides with the measured one. The positions of local minima of the spectra and, thus, the durations of all three pulses also agree very well (Fig. 7d).

The effect of filtering and a more detailed comparison of the peak positive pressure and duration of the measured and modeled signals over propagation distances are presented in Figs. 8a and 8b. The difference in peak positive pressure between the calculated signal (the solid line) and the measured one (the dotted line with cross marker) becomes almost negligible after applying the amplitude frequency filter to the calculated waveform (the circles). As has been already shown, the duration of the wave does not change with filtering. This can be seen in Fig. 8b, where the pulse half-durations extracted from filtered (the circles) and nonfiltered (the solid line) waveforms coincide with each other. A very good agreement between the results of numerical modeling with additional filtering and the laboratory-scale experiment data is obtained for the main shock pulse parameters. A small discrepancy in half-duration of the experimental (the cross markers) and theoretical pulses is observed due to the experimental error, i.e., generation of sparks with a slight difference in duration.

5. CONCLUSIONS

Nonlinear propagation of short-duration (30 μs) and high-amplitude (1100 Pa at 15 cm from the source) N-waves in a homogeneous standard atmosphere was studied numerically and experimentally. The Burgers equation extended to describe nonlinear spherically divergent waves in relaxing media was employed in the numerical analysis. Numerical simulations performed with alternative inclusion of different physical effects showed the relative importance of thermoviscous absorption, relaxation, and acoustic nonlinearity on the N-waveform distortion for the conditions of the laboratory experiment. Nonlinear effects were shown to be dominant in the pulse lengthening, whereas the peak positive pressure proved to depend on both nonlinear absorption and linear relaxation/absorption phenomena.

Absolute calibration of the amplitude and duration of pulses generated experimentally was performed. The pulse duration was defined from the position of the first nulls in the spectra of the measured signal. The peak pressure was calculated by matching the experimental and analytic curves of nonlinear N-pulse lengthening over the propagation distances. Nonlinear modeling of the N-pulse propagation was performed for the experimental conditions. Some distortion of the measured signals, as compared to the modeling waveforms, occurred due to the limited bandwidth of the measuring track. The distortion mainly consisted of a change in the peak pressure of the pulse, a broadening of the rise time of the shock front, and the appearance of additional oscillations.

The total frequency response of the measuring track was calculated as a ratio between the spectra of experimental and calculated signals and found to be close to the response of the microphone itself provided by the manufacturer. The frequency response has a plateau up to 10 kHz and a cutoff at about 150–200 kHz. Application of the calculated amplitude response to the numerical waveforms resulted in an even better agreement between simulations and experiment. Application of an appropriate phase frequency response could further advance the filtering procedure, but an improvement of the source pulse to pulse stability needs to be done, as well as more accurate measurements of the propagation distance, to define the calculated phase response more accurately.

The numerical analysis showed that, for the experimental setup used, nonlinear effects can not be neglected up to the distances of 2 m, at which the pressure level is higher than 70 Pa. This remark is very important for scale experiments designed to simulate the sound propagation in halls or streets, because nonlinear effects are usually not wanted for these applications [17]. On the other hand, it is possible to extend this developed and calibrated experimental setup to investigate nonlinear shock wave fields in turbulent media, as it would be for sonic boom outdoor propagation. In laboratory-scale experiments performed by two of the present authors, it was found that the first caustics (regions of focusing) in the field of N-waves propagating through turbulence are formed at distances of 1–1.2 m [11]. According to our results, nonlinear effects are still strong at these distances, which enables us to investigate nonlinear pulse propagation through caustics. To increase the distance of nonlinear propagation up to the second or third caustics, a more powerful spark source is required, or laser-generated N-waves can be used. The laser N-wave generation has been reported to produce a positive peak pressure as high as 2500 Pa at a distance of 20 cm from the source [2]. The numerical and experimental results obtained in this paper for N-wave propagation in a homogeneous atmosphere are shown to be in a good agreement, thus validating the model, the numerical algorithm, the filtering, and the calibration methods. A future work will extend the results to the case of nonlinear N-wave propagation in the presence of turbulence.

ACKNOWLEDGMENTS

REFERENCES

1. Ph. Blanc-Benon, B. Lipkens, L. Dallois, et al., J. Acouts. Soc. Am. **111** (1), 487 (2002).

2. Q. Qin and K. Attenborough, Appl. Acoust. **65**, 325 (2004).

3. B. Lipkens and D. T. Blackstock, J. Acoust. Soc. Am. **103**, 148 (1998).

4. H. E. Bass, R. Raspet, J. P. Chambers, and M. Kelly, J. Acoust. Soc. Am. **111**, 481 (2002).

5. V. I. Tatarskiĭ, *Wave Propagation in a Turbulent Atmosphere* (Nauka, Moscow, 1967) [in Russian].

6. O. V. Rudenko, A. K. Sukhorukova, and A. P. Sukhorukov, Akust. Zh. **40**, 290 (1994) [Acoust. Phys. **40**, 264 (1994)].

7. M. V. Aver'yanov, V. Khokhlova, O. A. Sapozhnikov, et al., Akust. Zh. **52**, 725 (2006) [Acoust. Phys. **52**, 623 (2006)].

8. R. O. Cleveland, J. P. Chambers, R. Raspet, et al., J. Acous. Soc. Am. **100**, 3017 (1996).

9. B. A. Davy and D. T. Blackstock, J. Acoust. Soc. Am. **49**, 732 (1971).

10. W. M. Wright, J. Acoust. Soc. Am. **73**, 1948 (1983).

11. S. Ollivier and Ph. Blanc-Benon, in *Proceedings of the 10th AIAA/CEAS Aeroacoustics Conference, Manchester, United Kingdom, 2004*, AIAA-2004-2921.

12. O. V. Rudenko and S. I. Soluyan, *Theoretical Foundations of Nonlinear Acoustics* (Nauka, Moscow, 1975; Consultants Bureau, New York, 1977).

13. R. O. Cleveland, M. F. Hamilton, and D. T. Blackstock, J. Acous. Soc. Am. **99**, 3312 (1996).

14. A. D. Pierce, *Acoustics*: *An Introduction to Its Physical Principles and Applications* (Acoust. Soc. Am., New York, 1989).

15. A. R. Kurganov and E. Tandmor, J. Comp. Phys. **160**, 241 (2000).

16. A. L. Polyakova, S. Soluyan, and R. V. Khokhlov, Akust. Zh. **8**, 107 (1962) [Sov. Phys. Acoust. **8**, 78 (1962)].

17. J. Picaut and L. Simon, Appl. Acoust. **62**, 327 (2001).